The Real-time Tracking Servo Control of a Rodless Pneumatic Actuator System under an Asymmetrical Load via the Feedback Measurement System

Hao-Ting Lin
Department of Mechanical and Computer-Aided Engineering, Feng Chia University, No. 100, Wenhwa Road, Seatwen, Taichung 40724, Taiwan, ROC

Keywords: Rodless Pneumatic Cylinder, Asymmetrical Load, Feedback Measurement System, Real-time Control, Path Tracking Servo Control.

Abstract: Due to the nonlinear and time-varying characteristics, pneumatic servo control systems are difficult to realize real-time path tracking control, especially for the rodless pneumatic cylinder which has relative larger friction force. An asymmetrical vertical load resulting from the gravity makes the motion control in the vertical direction more difficult. This study develops a rodless pneumatic actuator system for the real-time tracking servo control with an asymmetrical vertical load. First, the dynamic models of the rodless pneumatic actuator system will be established and simulated by the Matlab software. Then, the test rig layout will be proposed and experimented under the asymmetrical load via the feedback measurement system. Finally, the experimental results show that a rodless pneumatic actuator system with the asymmetrical vertical load is successfully implemented for the path tracking profile.

1 INTRODUCTION

The pneumatic system is one of the power sources to perform in the industry. Due to its reliability, low cost, cleanness, simplicity, easy maintenance, and safety in operation, the pneumatic system has gradually been widely adopted in the industrial automation. In recent years, pneumatic actuators have been used to work on positioning and motion tasks, and quite suitable for applying in the robotics fields. However, compared with electrical motors with equal power, pneumatic actuators are still not competitive in a few applications which demand accuracy, versatility and flexibility. Although pneumatic actuators have disadvantages such as high nonlinearity, low natural frequency due to low stiffness of air compressibility, and control complexity, researches on robots with the pneumatic actuator system are still popular in the automation industry.

Because pneumatic system is a highly nonlinear system and does not easily get accurate mathematical models, it is difficult and complicated to accomplish the pneumatic servo control (Oyama et al, 1990). To resolve the above problems, some researcher adopted the model reference control scheme (Gyeviki et al, 2005). In additional, Chiang and Lin proposed a Fourier series-based adaptive sliding-mode controller with H-inf tracking performance for the rodless pneumatic cylinder system (Chiang and Lin, 2011). The proposed method can not only be effective in preventing approximation errors, disturbance, and un-modeled dynamics, but it also guarantees a desired H-inf tracking performance for the overall system.

In this paper, the rodless pneumatic actuator is set up in the vertical direction to be an asymmetrical load mechanism system. For this system, the properties of mass, flow and pressure between two chambers of the pneumatic actuator are totally different while the pneumatic actuator works. These properties affect the overall system dramatically and the real-time control for the path tracking servo control is more difficult. In this research, the Matlab simulation will be establish to simulate the proposed system via the mathematical models and control methods. Finally, the test results indicate that the rodless pneumatic actuator system with an asymmetrical vertical load can follow the desired path profiles and achieve the required accuracy.

Lin, H-T.
The Real-time Tracking Servo Control of a Rodless Pneumatic Actuator System under an Asymmetrical Load via the Feedback Measurement System.
DOI: 10.5220/0005950603990403
In *Proceedings of the 13th International Conference on Informatics in Control, Automation and Robotics (ICINCO 2016) - Volume 1*, pages 399-403
ISBN: 978-989-758-198-4

2 DESCRIPTION OF THE SYSTEM

Figure 1 photographically shows the test rig of the rodless pneumatic servo system with an asymmetrical vertical load. The test rig layout is shown in Figure 2. In Figure 2, the real-time control of the rodless pneumatic actuator system mainly has five parts which are an air source unit, a rod-less pneumatic actuator, a proportional servo valve, signal processing cards and a PC-based controller unit. The air pressure for the experiments is set as 0.5 MPa. The rod-less pneumatic actuator and the proportional servo valve are manufactured by FESTO. The type of the rod-less pneumatic actuator is DGC-25-500-KF-YSR-A and the model of the pneumatic proportional servo valve is MPYE-5-M5-010-B. An optical linear encoder has a resolution of 0.1 μm for the feedback measurement system. The PC-based controller is a feedback measurement control unit which handles the control signals for the pneumatic proportional servo valve by an AD/DA interface card and gathers the feedback measuring signals for itself via a counter card. The control software of the overall system is computed by a 32-bit Open Watcom C program and the sampling frequency is 1000 Hz.

Figure 1: Rodless pneumatic actuator system.

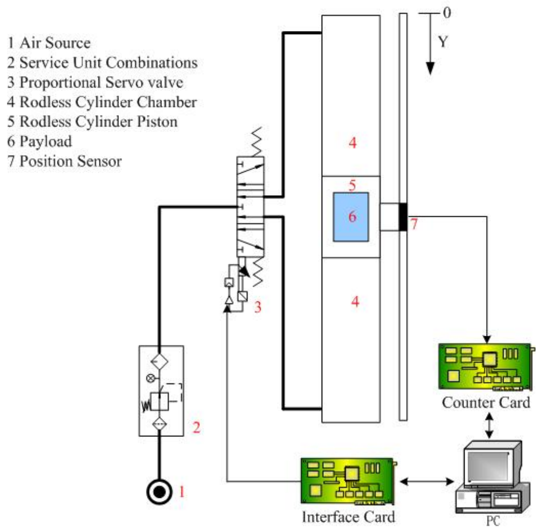

Figure 2: Test rig layout.

3 DYNAMIC MODELS AND THE CONTROL STRATEGY OF A RODLESS PNEUMATIC ACTUATOR SYSTEM WITH AN ASYMMETRICAL VERTICAL LOAD

In this research, the rodless pneumatic actuator is arranged in the vertical direction for the path tracking servo control. In this case, the gravity effect plays an important role in the rodless pneumatic actuator system with a vertical load. Therefore, the proposed system is an asymmetrical system when the block shifts dynamically in the rodless pneumatic actuator. The block motion in the pneumatic cylinder can dramatically influence the air flow rates and pressure changes between two cylinder chambers. In this chapter, the nonlinear mathematical models of the asymmetrical rodless pneumatic actuator system is derived inclusive of the dynamics of pneumatic servo valve, the mass flow rate equation of the pneumatic cylinder, the continuity equation and the motion equation. To implement the real-time servo control of a rodless pneumatic actuator system under an asymmetrical load, a Fourier series-based adaptive sliding mode controller with H-inf tracking performance (FSBASMC+Hinf) [3] is used for the overall feedback measurement system in this study.

3.1 The Dynamics of the Pneumatic Servo Valve

A proportional directional flow control valve is used in this experiment. The main feature of this type of valve is that its input control signal and the valve spool position is in the linear relationship. Hence, the dynamics of the valve can be described by the following relation:

$$X(t) = K_v(u(t) - u_n(t)) \tag{1}$$

where $X(t)$ is the valve spool displacement of the pneumatic servo valve, K_v represents the displacement-voltage gain, $u(t)$ is the control input and $u_n(t)$ is the neutral voltage.

3.2 The Mass Flow Rate Equation of the Pneumatic Cylinder

The mass flow rate of the air is dependent on the orifice area, temperature and pressure difference across the orifice, when the air flows through an orifice. In Figure 2, considering the mass flow rate of pneumatic cylinder chambers A and B, the following equation can be expressed as

$$\dot{m}(t) = \frac{C_d C_0 w X(t) P_u(t) \tilde{f}(p_r(t))}{\sqrt{T_u}} \tag{2}$$

where C_d is the discharge coefficient ($C_d = 0.8$), C_0 is the mass flow parameter, w is the port width (m), $P_u(t)$ is the up-stream pressure (N/m^2), T_u is the up-stream temperature, $p_r(t) = \frac{P_d(t)}{P_u(t)}$ is the ratio between the down-stream and up-stream pressure, $P_d(t)$ is the down-stream pressure (N/m^2), and

$$\tilde{f}(p_r(t)) = \begin{cases} 1, & \frac{P_{atm}}{P_u(t)} < p_r(t) < C_r \\ C_k\left[p_r^{\frac{2}{k}}(t) - p_r^{\frac{k+1}{k}}(t)\right]^{\frac{1}{2}}, & C_r < p_r(t) < 1 \end{cases} \tag{3}$$

For air, k =1.4 is the specific heat constant, C_r =0.528 and C_k =3.864. In order to simplify the analysis, the following functions can be derived as

$$\hat{f}(P_a(t), P_s(t), P_e(t)) = \begin{cases} \dfrac{P_s(t)\tilde{f}(\frac{P_a(t)}{P_s(t)})}{\sqrt{T_s}} \\ \dfrac{P_a(t)\tilde{f}(\frac{P_e(t)}{P_a(t)})}{\sqrt{T_a}} \end{cases} \tag{4}$$

$$\hat{f}(P_b(t), P_s(t), P_e(t)) = \begin{cases} \dfrac{P_b(t)\tilde{f}(\frac{P_e(t)}{P_b(t)})}{\sqrt{T_b}} \\ \dfrac{P_s(t)\tilde{f}(\frac{P_b(t)}{P_s(t)})}{\sqrt{T_s}} \end{cases} \tag{5}$$

where P_s =5x10^5 (N/m^2) is the supply pressure, P_e =1 x10^5 (N/m^2) is the exhaust pressure, P_a and P_b are the pressure values of the chamber A and B, T_s =293K is the supply temperature, T_a and T_b are the temperature values in the chamber A and B.

3.3 The Continuity Equation

We assume that the air into the cylinder is an adiabatic process of an ideal gas, the change in energy can be shown as

$$\frac{d}{dt}(c_v \rho_c V(t) T_s) = \dot{m}(t) C_P T_s - P(t)\dot{V}(t) \tag{6}$$

where c_v is the specific heat of air at constant volume, ρ_c is the air density of the cylinder, $V(t)$ is the volume of the cylinder, $\dot{m}(t)$ is the mass flow rate, C_P is the specific heat of air at a constant pressure and $P(t)$ is the pressure of the chamber. Assuming an ideal gas

$$\begin{aligned} \dot{m}(t) &= \frac{\frac{d}{dt}(c_v \rho_c V(t) T_s) + P(t)\dot{V}(t)}{C_P T_s} \\ &= \frac{\dot{P}(t)V(t)}{kRT_s} + \frac{P(t)\dot{V}(t)}{kRT_s} + \frac{P(t)\dot{V}(t)}{C_P T_s} \end{aligned} \tag{7}$$

where $k = \frac{C_P}{c_v}$ is the ratio of the specific heat for air at the temperature T_s. For an ideal gas

$$\frac{1}{R} = \frac{1}{C_P} + \frac{1}{kR} \tag{8}$$

where R=287 (J/kg*K) is the universal gas constant. Then

$$\dot{m}(t) = \frac{\dot{P}(t)V(t)}{kRT_s} + \frac{P(t)\dot{V}(t)}{RT_s} \tag{9}$$

For the chamber A and B, the following equations hold:

$$\dot{m}_a(t) = \frac{\dot{P}_a(t)V_a(t)}{kRT_s} + \frac{P_a(t)\dot{V}_a(t)}{RT_s} \tag{10}$$

$$\dot{m}_b(t) = \frac{\dot{P}_b(t)V_b(t)}{kRT_s} + \frac{P_b(t)\dot{V}_b(t)}{RT_s} \tag{11}$$

where V_a and V_b are the volumes of the chamber A and B. Combining Eqs. (2)-(5), (10) and (11) as

$$\dot{P}_a(t) = \frac{kRT_s C_d C_0 w X(t)\hat{f}(P_a(t), P_s(t), P_e(t)) - kP_a(t)\dot{V}_a(t)}{V_a(t)} \tag{12}$$

$$\dot{P}_b(t) = \frac{kRT_s C_d C_0 w X(t)\hat{f}(P_b(t), P_s(t), P_e(t)) - kP_b(t)\dot{V}_b(t)}{V_b(t)} \tag{13}$$

3.4 The Motion Equation

Applying the Newton's second law of motion, the asymmetric pneumatic cylinder's motion can be described as

$$\begin{aligned}&(AP_a(t) - AP_b(t))\operatorname{sgn}(x(t)) - K_f\dot{x}(t)\\&-K_{S-c}(x(t))S(\dot{x}(t), P_a(t), P_b(t)) - Mg = M\ddot{x}(t)\end{aligned} \tag{14}$$

where A denotes the piston area (m^2), M is the mass (kg), Mg indicates the asymmetrical vertical payload, K_f is the viscous friction coefficient, and $K_{S-c}(x)$ is the combination of static and Coulomb friction forces which are position and velocity dependent. Function is expressed as

$$K_{S-c}(x(t))S(\dot{x}(t), P_a(t), P_b(t))$$

$$K_{S-c}(x(t))S(\dot{x}(t), P_a(t), P_b(t)) = \begin{cases} AP_a(t) - AP_b(t), \\ as\,\dot{x} = 0\, and \left|AP_a(t) - AP_b(t)\right| \le K_S(x(t)) \\ K_c(x(t))\operatorname{sgn}(\dot{x}(t)), \\ as\,\dot{x} \ne 0\, or \left|AP_a(t) - AP_b(t)\right| > K_S(x(t)) \end{cases} \tag{15}$$

where $K_S(x(t))$ is the position-dependent static frictions, $K_c(x(t))$ is the variable position-dependent load via friction effects.

Furthermore, $V_a(t)$ and $V_b(t)$ are defined as

$$V_a(t) = A(x(t) + \Delta) \tag{16}$$

$$V_b(t) = A(l - x(t) + \Delta) \tag{17}$$

where l is the stroke (m), Δ is an equivalent extra length to the cylinder.

3.5 Control Strategy

The block diagram of the overall scheme is shown in Figure 3. To realize the real-time path tracking servo control for the rodless pneumatic actuator system under an asymmetrical load, the FSBASMC-Hinf is adopted in this study. Define the output error as

$$e(t) = y(t) - y_m(t) \tag{18}$$

where $y_m(t)$ is a given bounded reference signal. The sliding surface is described as

$$s = a_1 e(t) + a_2\dot{e}(t) + \ldots + e^{(n-1)}(t) \tag{19}$$

where a_i are chosen such that $\sum_{i=1}^{n} a_i\lambda^{i-1}$ is a Hurwitz polynomial. In this paper, the FSBASMC-Hinf controller is proposed to solve the high non-linearity and time-varying problems of the rodless pneumatics servo system under the asymmetrical load. Therefore, the control input is chosen as

$$u = \frac{-\hat{\mathbf{W}}_F^T\mathbf{q}_F(t) - a_1\dot{e} - a_2\ddot{e} - p_{21}e - p_{22}\dot{e} + y_m^3(t) - \dfrac{s}{2\rho^2}}{\hat{\mathbf{W}}_G^T\mathbf{q}_G(t)} \tag{20}$$

where the sliding surface defined as $s = \ddot{e} + 5\dot{e} + 40e$, initial values of Fourier coefficients $\hat{\mathbf{W}}_F$ and $\hat{\mathbf{W}}_g$ are $[0, 0, \cdots, 0]_{1\times 11}$ and $[20000, 0, \cdots, 0]_{1\times 11}$, respectively, a_1 is 40, a_2 is 5 and $\rho = 0.2$.

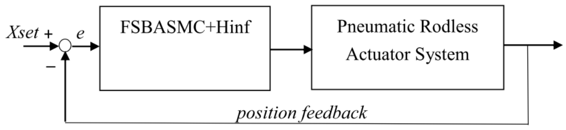

Figure 3: The block diagram of the overall scheme.

4 SIMULATIONS AND EXPERIMENTS

First, the simulation of the overall rodless pneumatic actuator system is established by the Matlab software. Next the experiments of path tracking servo control in a rodless pneumatic system under an asymmetrical load are implemented. In the experiments, the desired path trajectory, namely a fifth-order polynomial function is chosen for the real-time path tracking servo control in the vertical direction.

4.1 Simulations of Path Control

The simulation of the path tracking servo control of a fifth order polynomial with stroke of 200 mm in 2 sec controlled by FSBASMC+Hinf is implemented, as shown in Figure 4, where the position control response, the control error and the control input are schematically described. The simulation responses by FSBASMC+Hinf are shown in Figure 4(a). From Figure 4(b), the tracking error is bounded and well converged. Figure 4(c) shows the control signal of FSBASMC+Hinf.

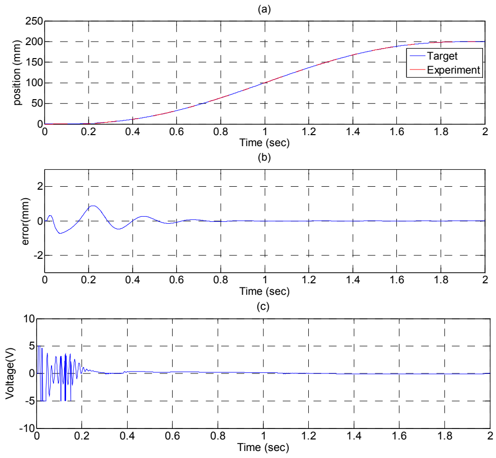

Figure 4: Simulation results of the rodless pneumatic actuator system under an asymmetrical load for a fifth order polynomial path with stroke of 200 mm in 2 sec: (a) position control response (b) control error (c) control input.

4.2 Experiments of Path Control

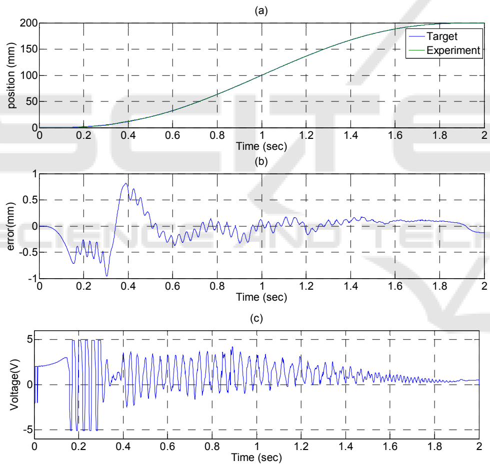

Figure 5: Experimental results of the rodless pneumatic actuator system under an asymmetrical load for a fifth order polynomial path with stroke of 200 mm in 2 sec: (a) position control response (b) control error (c) control input.

In the experiments, the position responses, tracking errors and control inputs for the rodless pneumatic actuator system under an asymmetrical load by a fifth order polynomial with stroke of 200 mm in 2 sec are shown in Figure 5. Figure 5(b) shows the maximum tracking error can reach about 0.9mm. The control inputs are shown in Figure 5(c). From Figure 5(c), control input signals fluctuate form +5 volts to -5 Volts. Therefore, the desired tracking performance can be achieved.

5 CONCLUSIONS

In this study, a rodless pneumatic actuator system under an asymmetrical load has been developed and successfully implemented for real-time path tracking servo control by the feedback measurement system. The dynamic models and the control strategies are built in Matlab software. The real-time control measurement system is established by PC-based system. For further confirming the proposed system, the 5-th order polynomial path is implemented. Finally, the simulation and experimental results demonstrate that the proposed method is validated to apply in the real-time path tracking control of the pneumatic servo system under the asymmetrical vertical load.

ACKNOWLEDGEMENTS

This research was sponsored by Ministry of Science and Technology, Taiwan under the grant MOST 104-2218-E-035 -017.

REFERENCES

Oyama, O. et al, 1990. Model reference adaptive control for a pneumatic cylinder servo system. *Journal of the Japan Hydraulic Pneumatic Society,* Vol. 21, pp. 182-186.

Gyeviki, J. et al, 2005. Sliding Modes Application in Pneumatic Positioning. *Proceedings of the 2005 IEEE International Conference on Mechatronics*, Taipei, Taiwan, pp. 964-969, July 10-12.

Chiang, M. H., Lin, H. T., 2011. Development of a 3D parallel mechanism robot arm with three vertical-axial pneumatic actuators combined with a stereo vision system. *Sensors*, Vol. 11, pp. 11476-11494.